This article has been accepted for publication in a future issue of this journal, but has not been fully edited. Content may change prior to final publication. Citation information: DOI 10.1109/TEC.2017.2758382, IEEE Transactions on Energy Conversion

Analytic Model for Induction Motors under Localized Bearing Faults

Mansour Ojaghi, *Member, IEEE*, Mahdi Sabouri, and Jawad Faiz, *Senior Member, IEEE*

***Abstract*— The bearing faults are the major root cause for the induction motor failures; however, almost all the related fault diagnosis methods have been based on the laboratory tests, which are costly and inflexible. Localized defects in various components of roller bearings cause radial vibration of the rotor, little variation of the load torque and various harmonics in the stator current. Ignoring the load torque variation, this paper applies the multiple coupled circuit modeling to simulate three-phase squirrel-cage induction motors under the localized bearing faults by introducing appropriate air gap function. Fast Fourier transform is used for exact analysis of the harmonic content of the inverse of the air gap function. The analysis is completed by including the saturation effect and the inherent eccentricity of the motor. Then, a broad list of harmonics presentable in the stator current spectrum under the bearing faults is determined. The list may include the characteristic vibration frequencies related to the bearing components faults. Also, it is clear that the inner raceway fault can produce the same harmonics in the stator current as produced by the mixed eccentricity. Experimental results approve the simulation results and the mentioned facts.**

***Index Terms*—Analytic model, induction motor, localized bearing faults, modified winding function theory, roller bearing, simulation**

I. INTRODUCTION

THREE phase squirrel cage induction motors (SCIMs) have found wide applications because of their low cost, simple and rugged construction, wide range of speed and some other benefits. Condition monitoring for detecting incipient faults is essential for the motors, especially at high power ratings, where it is not easy to replace the faulty motor and the repair takes long time and high cost. Losses due to cessation of production line should be added to the mentioned costs. Using condition monitoring technologies, the incipient faults can be detected and removed prior to their extension as major damages of the motor. Early detection of the faults in SCIMs can involve the following advantages:

- Preventing major damages to the motor, and costly and long time repairs.
- Avoiding unexpected stop of the production line.
- Reducing losses and wasting products.

Achieving above benefits requires the knowledge of the extent and location of the incipient faults in the motor.

Bearings are exposed to the failure in SCIMs. The bearing failure could be the origin for some other faults within the motor. About 40% - 50% of total failures of SCIMs are related to their bearing faults [1]. The reason is that even in normal operation with balanced and aligned load with the rotor shaft, mechanical fatigue damages the bearing components. Bearings have a lot of talents to deteriorate due to their continuous operation under various stresses. However, if the process of creation and development of bearing defects can be revealed at an early stage, the significant failures of the motor and the losses caused by an unexpected stop of the motor can be prevented.

Roller bearing defects may be categorized as distributed or localized defects. Distributed defects include surface roughness, waviness, misaligned races and off-size rolling elements. Localized defects include cracks, pits and spalls on the rolling surfaces [2]. Bearing faults may be originated from the localized defects on the bearing inner raceway, outer raceway or balls. Passing the balls through the defect location causes generating thuds in the motor vibration signal whose amplitude depend on the defect extent and location as well as the clearance between the bearing components. The period of occurrence of the thuds depend on the shaft speed as well as the faulty component and physical dimensions of the bearing. According to this fact, vibration frequency components have often been used for bearing fault diagnosis purposes [2]-[5].

The vibration frequency components due to the bearing faults are also reflected in the stator line current, so, the motor current signature analysis (MCSA) can be used for the bearing fault diagnosis purposes. As the stator current signals are measured more easily and reliably, recent researches on the topic are conducted toward using MCSA approaches [6]-[8]. Based on the radial rotor movement and the load torque variations caused by the bearing localized defects, new expressions have been given for the stator current frequency content due to the bearing defects in [9]. In [10], the bearing fault detection of a three-phase induction motor was performed by analyzing the squared envelope spectrum of the stator current, where spectral kurtosis-based algorithms are also applied to improve the analysis. A combined fast Fourier

M. Ojaghi and M. Sabouri are with the Department of Electrical Engineering, University of Zanjan, Zanjan, Iran (email: mojaghi@zun.ac.ir & m.sabouri@znu.ac.ir).

J. Faiz is with the Center of Excellence on Applied Electromagnetic Systems, School of Electrical and Computer Engineering, College of Engineering, University of Tehran, Tehran, Iran (email: jfaiz@ut.ac.ir).

This article has been accepted for publication in a future issue of this journal, but has not been fully edited. Content may change prior to final publication. Citation information: DOI 10.1109/TEC.2017.2758382, IEEE Transactions on Energy Conversion

transform and support vector machine (SVM) technique was used for selection of the stator current frequencies related to the bearing localized faults in [11]. A pattern recognition approach for the bearing fault detection in induction motors has been achieved in [12] by combining the stationary wavelet packet transform and the directed acyclic graph SVM. A root-multiple signal classification method has been introduced for identification of the progressive cracking in the bearing of the induction motors in [13], whose main advantage is the very good frequency resolution for a very short acquisition time. Reference [14] has focused on the bearing fault detection in induction machines based on the stator currents analysis using the Hilbert–Huang transform. The influence of external radial load applied to the shaft on the bearing fault detection of the induction motors based on vibration or current signals has been investigated in [15]. A bearing fault diagnosis method based on large memory storage retrieval neural networks using acoustic emission (AE) sensors has been presented in [16], where the AE signals are preprocessed with the simple short-term Fourier transform (STFT).

While the bearing faults are the major reasons for the failure of the SCIMs, almost all the related fault diagnosis methods have been based on the laboratory test results, which are costly and inflexible, so, the need for accurate modeling and simulation of the SCIMs under the bearing faults is fully sensible. Winding function approach has been used in [17], [18] to model and simulate an SCIM with sleeve bearings under the bearing oil-whirl fault condition. Reference [19] has focused on the air gap variation due to the ball bearing faults, where the fault has been modeled using contact mechanics that is rather complicated. A dynamic analytical model based on principles of generalized harmonic analysis and complex conductor distribution has been developed for wound rotor induction machines in [20] that accounts for air gap field disturbances introduced by the presence of a typical outer race bearing defect. Ignoring little load torque variation due to the bearing localized defects [9], the authors presented a paper [21], where the multiple coupled circuit method (MCCM) [22] has been applied to model and simulate three-phase SCIMs under localized bearing faults by using appropriate air gap functions.

This paper applies the same approach as applied in [21] with important new contributions including: a comprehensive analysis of harmonic content of inverse of the air gap function under various localized bearing defects by using the fast Fourier transform (FFT), including the saturation effect and the inherent eccentricity of the motor in the mentioned analysis, offering an analytical development to indicate how the air gap radial vibrations create harmonic components in the stator current, preparing a more general and comprehensive expression for the harmonic frequencies presentable in the stator current spectrum due to the localized bearing faults, including the saturation effect and inherent eccentricity in the modeling and simulation and supporting the modeling and simulation results with corresponding experimental results. The new expression for the stator current harmonics includes some new harmonics such as the characteristic vibration frequencies of the bearing defects. Also, using this expression, it becomes clear that the inner raceway fault can produce the same harmonics in the stator current as produced by the mixed eccentricity fault. The stator current spectra obtained through simulation under the outer raceway and inner raceway defects show many of the analytically predicted harmonics. Experimental results approve the simulation results and the mentioned facts.

The paper is organized as follows: roller bearing localized defects are introduced in section II. Calculation of various inductances of the SCIM under the localized bearing faults is explained in section III. Section IV gives the FFT analysis to determine the harmonic content of the inverse air gap function and the stator line current. Section V presents the experimental verification of the modeling and simulation results, and finally, section VI concludes the paper.

II. Localized Defects in Roller Bearings

Roller bearings comprise of the following components:

- The outer ring with a slot in its inner surface (outer raceway).
- The inner ring with a slot in its outer surface (inner raceway).
- The roller elements, which could be spherical (balls) or cylindrical.
- The cage that holds the roller elements at fixed spaces to each other.

Fig. 1 shows the geometry of a roller bearing with spherical balls (ball bearing). Local defect or abrasion causes periodic bumps on the motor vibration signal. Amplitude of the bumps depend on the defect extent and location, the clearance between the raceways and the balls and the clearance between the cage loops and the balls. Period of repetition of the bumps depend on the shaft speed, defective element of the bearing and its physical dimensions. Vibration frequency caused by local defect on a ball (f_b) is twice its frequency of rotation around itself and is calculated as follows [9]:

$$f_b = \frac{D_c}{D_b} f_r \left(1 - \frac{D_b^2}{D_c^2} \cos^2 \beta\right) \tag{1}$$

where f_r is the mechanical speed of the shaft in rps, D_b is the balls diameter, D_c is the cage diameter and β is the contact angle of the balls (see Fig. 1). Local defects on the outer and inner raceways cause vibrations whose frequencies, f_o and f_i, are calculated as follows [9]:

$$f_o = \frac{N_b}{2} f_r \left(1 - \frac{D_b}{D_c} \cos\beta\right) \tag{2}$$

$$f_i = \frac{N_b}{2} f_r \left(1 + \frac{D_b}{D_c} \cos\beta\right) \tag{3}$$

where N_b is the balls number. The rotor vibrations caused by the bearing faults create harmonic components in the stator line currents. Some expressions have been given for the frequencies of these harmonics in [6], [9]. Taking into account the core saturation effect and the inherent eccentricity of the motor, section IV gives a more general and comprehensive expression for the harmonics frequencies.

This article has been accepted for publication in a future issue of this journal, but has not been fully edited. Content may change prior to final publication. Citation information: DOI 10.1109/TEC.2017.2758382, IEEE Transactions on Energy Conversion

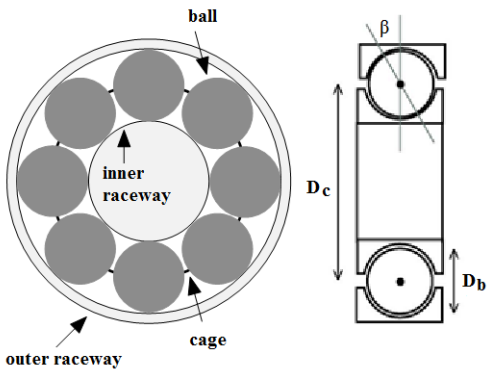

Fig. 1. Geometry of a ball bearing

III. Inductances Calculation under Bearing Defects

MCCM in the SCIMs usually includes three dynamic voltage equations for the stator windings, *R* number of dynamic voltage equations for the rotor meshes; actually, *R* is the number of the rotor bars, and two mechanical dynamic equations for rotation of the rotor. These, dynamic equations as well as a simple numerical method to solve them are given in [21]. Calculation of various self/mutual inductances of the motor at every new position of the rotor is an essential step when solving the equations. Modified winding function theory (MWFT) is used for calculating the inductances under different localized bearing defects [23]. In order to use MWFT, turn functions and modified winding functions of the rotor and stator circuits as well as the motor air gap function should be determined under the bearing defects. Figs. 2 shows the radial motion of the shaft and the resultant temporary eccentricity due to the local defects on the outer and inner raceways. When no ball is at the defect position (for $t \neq k/f_{ch}$; k=1,2,3,…), the air gap length is the same around the rotor as with the healthy bearings, where f_{ch} is equal to f_o, f_i or f_b corresponding to the defective element of the bearing. However, when $t=k/f_{ch}$, the air gap length distribution will temporarily be non-uniform due to pass of a ball through the defect position. Therefore, using the unit impulse function δ( ), the air gap length distribution under the bearing localized defects can be expressed as follows [9]:

$$g(\varphi,t) = g_0[1-\rho\cos(\varphi-\psi(t))\sum_{k=-\infty}^{\infty}\delta(t-\frac{k}{f_{ch}})] \quad (4)$$

where g_0 is the uniform air gap length in the healthy condition, ρ is the temporary eccentricity degree caused when passing the balls through the defect position, φ is the angle in the stator reference and $\psi(t)$ equals to 0, $\omega_i t$ and $\omega_{cage} t$ for outer raceway, inner raceway and ball defects respectively and ω_{cage} is the cage speed, which is calculated as follows [24]:

$$\omega_{cage} = \frac{\omega_r}{2}(1-\frac{D_b}{D_c}\cos\beta) \quad (5)$$

Using (4) and MWFT, any self/mutual inductance of the SCIM is calculated by the following integral equation [23]:

$$L_{xy} = \mu_o r l \int_0^{2\pi} n_x(\varphi) N_y(\varphi) g^{-1}(\varphi,t) d\varphi \quad (6)$$

where *x* and *y* should be replaced by any phase or mesh of the stator and rotor, μ_0 is the air magnetic permeability, *r* is the air gap mean radius, *l* is the stack length, $g^{-1}(\varphi,t)$ is the inverse of the air gap function, $n_x(\varphi)$ is the *x* phase (mesh) turn function and $N_y(\varphi)$ is the *y* phase (mesh) modified winding function that is defined by:

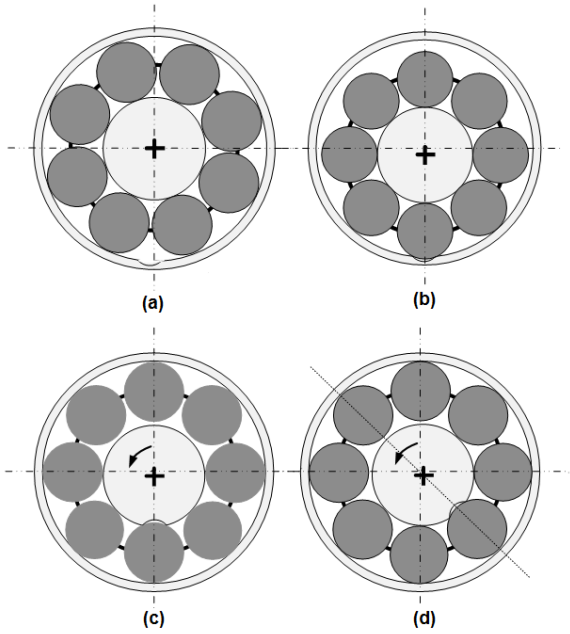

Fig. 2. (a) Uniform air gap when no ball passes through the defect position, (b) temporary eccentricity at fixed position when passing the balls through the outer raceway defect position, (c) temporary eccentricity when passing a ball through the inner raceway defect position, (d) changing the position of the temporary eccentricity by rotation of the shaft for the inner raceway defect

$$N_y(\varphi) = n_y(\varphi) - \frac{< g^{-1}(\varphi,t) n_y(\varphi) >}{< g^{-1}(\varphi,t) >} \quad (7)$$

where < > shows an averaging operator, such that $< f >$ is the average of the function *f* in the range from 0 to 2π as follows:

$$< f(\varphi) > = \frac{1}{2\pi}\int_0^{2\pi} f(\varphi) d\varphi \quad (8)$$

Fig. 3 shows the time variation of the self-inductance of the stator phase "a" (L_{aa}) at healthy and outer raceway fault conditions. The figure is plotted during simulation processes of SCIM. As seen, small pulses of f_o frequency are created in the inductance value due to the outer race fault. Fig. 4 shows the time variation of mutual inductance between the stator phase "a" and the rotor mesh "1" (L_{a1}) at healthy and inner raceway fault conditions. This figure is also obtained during simulation processes. As seen, the raceway fault causes local deeps and spikes on the trace of the mutual inductance. Fig. 5 shows variation of self-inductance of the rotor mesh "1" (L_{11}) with time at healthy and ball defect conditions obtained by simulation. Local deeps and spikes are produced on the inductance trace at a frequency of f_b. Amplitude of the deeps and spikes are changed depending on the relative positions of the proposed mesh and the defective ball. In the simulations leading to Figs. 3-5, ρ=0.3 is applied to show qualitatively how different localized defects affect various inductances of the motor. Changing this value will result in changing magnitude of the resultant deeps and/or spikes on the inductance traces without changing their frequency of occurrence.

This article has been accepted for publication in a future issue of this journal, but has not been fully edited. Content may change prior to final publication. Citation information: DOI 10.1109/TEC.2017.2758382, IEEE Transactions on Energy Conversion

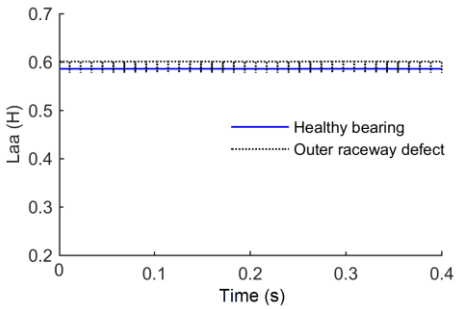

Fig. 3. Variation of the stator phase "a" self inductance with time under healthy and outer raceway defect conditions.

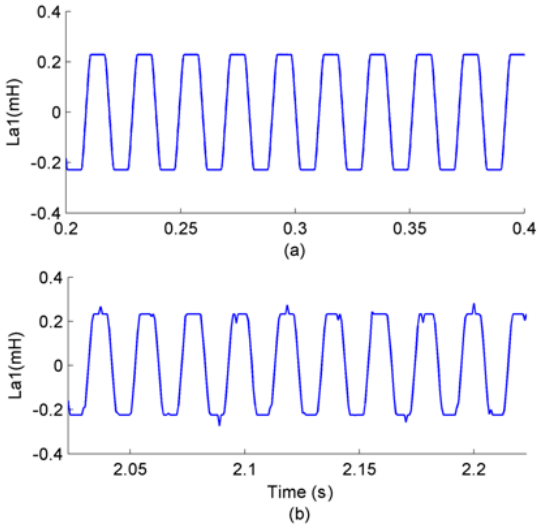

Fig. 4. Variation of the mutual inductance between the stator phase "a" and the rotor mesh "1" with time under: a) healthy, and b) inner raceway defect conditions.

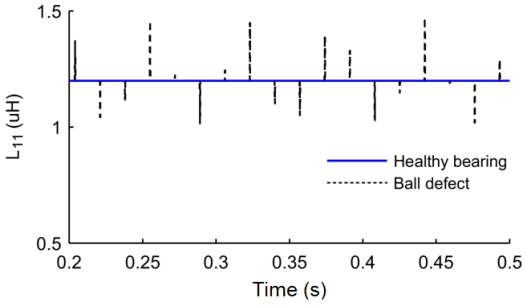

Fig. 5. Variation of the self inductance of the rotor mesh "1" with time under healthy and ball defect conditions

IV. Stator Current Harmonics Due to Bearing Defects

In operating motor the stator winding loops are closed through the voltage source, so, any induced voltage within the stator windings can produce its own current contribution. Regardless of polarity, a general expression for the induced voltage in the stator winding 'a' is attained by differentiating its total flux linkage (λ_{as}) versus time as follows:

$$e_{as} = \frac{d\lambda_{as}}{dt} \tag{9}$$

where λ_{as} is sum of contributions from all the stator winding and rotor mesh currents as follows [21]:

$$\lambda_{as} = \begin{bmatrix} L_{aa} & L_{ab} & L_{ac} \end{bmatrix} \begin{bmatrix} i_{as} & i_{bs} & i_{cs} \end{bmatrix}^T + \begin{bmatrix} L_{a1} & L_{a2} & \dots & L_{aR} \end{bmatrix} \begin{bmatrix} i_1 & i_2 & \dots & i_R \end{bmatrix}^T \tag{10}$$

where L_{aa} is the self inductance of the stator winding 'a', L_{ai} is the mutual inductances between the stator windings 'a' and the stator winding or rotor mesh 'i' (i=a, b, 1, 2, ..., R), i_{as}, i_{bs} and i_{cs} are the stator winding currents and i_j is the current of the rotor mesh 'j' (j=1, 2, ..., R). According to (6), any radial vibration of the inverse of the air gap function causes variation of the self/mutual inductances of the motor at the same frequency, say f_v. Figs. 3-5 approve this fact. On the other hand, the mains voltage usually is not purely sinusoidal and contains harmonics of kf_s frequencies (k=1,2, ...), which are reflected in the stator currents. Then, due to multiplication of the inductances to the stator currents in (10), λ_{as} will contain harmonics with $|kf_s \pm f_v|$ frequencies. Therefore, given the mains voltage fundamental frequency (f_s) and harmonic content, the stator current harmonics due to the faults are predicted by determining the harmonics of the inverse of the air gap function, i.e. the inverse of (4) as follows:

$$g^{-1}(\varphi,t) = \frac{1}{g_0[1-\rho\cos(\varphi-\psi(t))\sum_{k=-\infty}^{\infty}\delta(t-\frac{k}{f_{ch}})]} \tag{11}$$

While performing analytic Fourier analysis to determine the time harmonics of this function is so complicated, corresponding numerical analysis can be performed more easily using the fast Fourier transform (FFT). Assuming g_0=0.001 m, ρ=0.3, $\psi(t)$=$2\pi f_a t$ with f_a=19 rps and f_{ch}=130 Hz, function $g^{-1}(\varphi,t)$ is calculated at a fixed angle (φ=0) in a reasonable time span and time steps. Then, FFT is used to determine the frequency spectrum of the function. Fig. 6 shows the time trend of the resultant inverse air gap function and its normalized frequency spectrum. As seen, the spectrum includes harmonics at cf_{ch}, af_a and $|cf_{ch} \pm af_a|$ frequencies (a,c=1,2,3,...).

For economic utilization of the magnetic material, the operating points of electrical machines may be extended above the knee of the magnetization characteristic, i.e. into the saturation. Under saturation, reluctance of the magnetic core increases and may not be ignorable. Therefore, the core reluctance can be substituted by a proportional increase in the air gap length along the main flux path [25], [26]. Since the increase of the magnetic core reluctance due to the saturation depends on the local flux density and is independent of the flux direction, it is expected that the resultant fictitious air gap length to fluctuate a complete cycle every half cycle of the air gap flux density around the air gap. Ignoring some higher order harmonics, an equivalent inverse air gap function under the mixed eccentricity fault and the magnetic saturation effect has been introduced in [27]. The same function is revised for the bearing localized defects as follows:

$$g^{-1}(\varphi,t) = \frac{1-k_n+k_n\cos[p(\varphi-\varphi_f)]}{g_0[1-\rho\cos(\varphi-\psi(t))\sum_{k=-\infty}^{\infty}\delta(t-\frac{k}{f_{ch}})]} \tag{12}$$

where φ_f is the air gap flux position which rotates by the mechanical synchronous speed (f_{sm} rps), p is the poles number and k_n is defined as follows [27]:

This article has been accepted for publication in a future issue of this journal, but has not been fully edited. Content may change prior to final publication. Citation information: DOI 10.1109/TEC.2017.2758382, IEEE Transactions on Energy Conversion

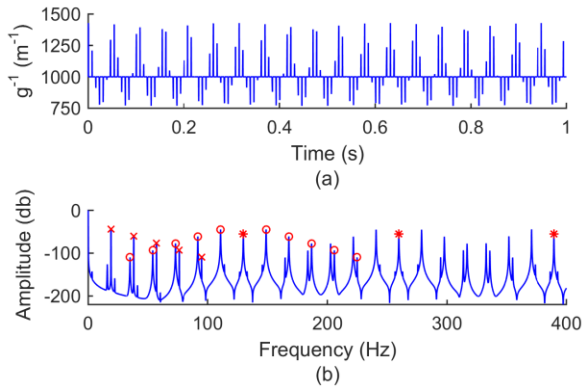

Fig. 6. The inverse air gap function under the bearing localized faults: (a) time trend, (b) frequency spectrum with indicated cf_{ch} (✱), af_a (×) and $f_{ch}\pm af_a$ (○) harmonics

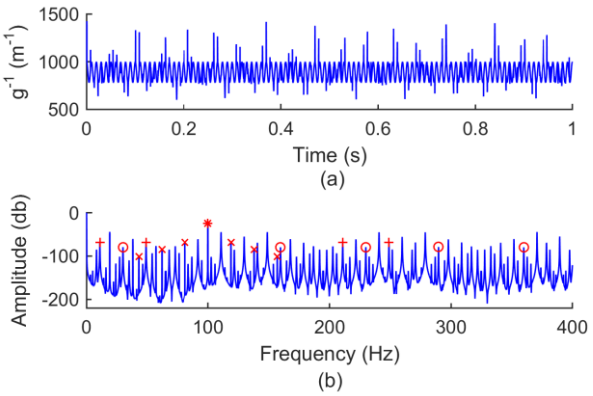

Fig. 7. The inverse air gap function under the bearing localized faults by including the saturation effect: (a) time trend, (b) frequency spectrum with indicated $2f_s$ (✱), $2f_s\pm af_a$ (×), $|2f_s\pm cf_{ch}|$ (○) and $|2f_s\pm cf_{ch}\pm f_a|$ (+) harmonics

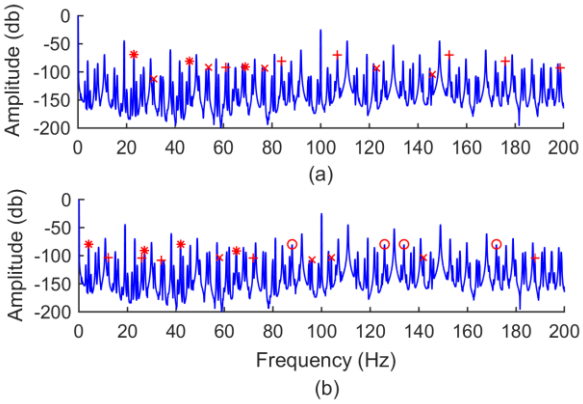

Fig. 8. The frequency spectrum of the inverse air gap function under the bearing localized faults by including the saturation effect and inherent eccentricity: (a) indicated rf_r (✱), $2f_s\pm rf_r$ (×) and $f_{ch}\pm rf_r$ (+) harmonics, (b) indicated $|rf_r\pm f_a|$ (✱), $2f_s\pm f_r\pm f_a$ (×), $f_{ch}\pm f_r\pm f_a$ (○) and $|f_{ch}\pm 2f_s\pm f_r\pm f_a|$ (+) harmonics

$$k_n = \frac{2(k_{sat}-1)}{3k_{sat}} \tag{13}$$

where k_{sat} is the saturation factor defined as follows [27]:

$$k_{sat} = \begin{cases} B_1/B_n ; & B_1 > B_n \\ 1 ; & B_1 \le B_n \end{cases} \tag{14}$$

where B_n is the knee point flux density of the core material and B_1 is magnitude of the space fundamental harmonic of the air gap flux density. Fig. 7 shows the time variation and frequency spectrum of the inverse air gap function with the same parameters by including the saturation effect with k_{sat}=1.2. As seen, besides the harmonics presented in Fig. 6b, a new harmonic component appears at $2f_s$ frequency. This is the result of multiplication of the number of the complete fluctuations of the fictitious air gap around the rotor due to saturation (p) by the speed of the air gap flux density that is $f_{sm}=2f_s/p$. In addition, the previous harmonics shown in Fig. 6b are reflected both sides this new harmonic as $|2f_s\pm cf_{ch}|$, $|2f_s\pm af_a|$ and $|2f_s\pm cf_{ch}\pm af_a|$ harmonics.

Due to some manufacturing tolerances, a small severity of eccentricity may exist even in the new machines, which is called the inherent eccentricity. By including the inherent eccentricity as well, the inverse air gap function of (12) is modified as follows:

$$g^{-1}(\varphi,t) = \frac{1-k_n+k_n\cos[p(\varphi-\varphi_f)]}{g_0[1-\rho_e\cos(\varphi-\varphi_m)-\rho\cos(\varphi-\psi(t))\sum_{k=-\infty}^{\infty}\delta(t-\frac{k}{f_{ch}})]} \tag{15}$$

where ρ_e and φ_m are the inherent eccentricity severity and the minimum air gap position due to the eccentricity, respectively. Assuming the position of the static component of the inherent eccentricity to be at φ=0, these parameters are defined as follows [27]:

$$\rho_e = \sqrt{\rho_s^2+\rho_d^2+2\rho_s\rho_d\cos\theta_r} \tag{16}$$

$$\varphi_m = \tan^{-1}\frac{\rho_d\sin\theta_r}{\rho_s+\rho_d\cos\theta_r} \tag{17}$$

where ρ_s and ρ_d are the static and dynamic components of the inherent eccentricity, respectively and θ_r is the rotor position angle. Using the same parameter values and putting ρ_s=0.02 and ρ_d=0.015, the time variation of the function (15) is calculated at the rotor speed of 23 rps (f_r=23 rps) and its frequency spectrum is determined and shown in Fig. 8. As seen, in addition to the previous harmonics, new harmonics are present in the spectrum whose frequencies include rf_r, $|2f_s\pm rf_r|$, $|cf_{ch}\pm rf_r|$, $|rf_r\pm af_a|$, $|2f_s\pm rf_r\pm af_a|$, $|cf_{ch}\pm rf_r\pm af_a|$ (r=1, 2, ...).

Therefore, by including saturation effect and inherent eccentricity, the inverse of the air gap function will contain many harmonics under the bearing localized defects. The frequencies of these harmonics are summarized as follows:

$$f_v = |sf_s \pm cf_{ch} \pm rf_r \pm af_a| \tag{18}$$

where a,c,r=0,1,2,... and s=0,2. Putting any of the parameters s, c, r and a equal to zero in (18), does not mean that the related phenomenon has been neglected, but it merely means that it is to consider some frequencies that they do not depend on this phenomenon. As mentioned before, by modulating the stator supply harmonics, the resultant harmonics in the stator line current will be as follows:

$$f_{cur} = |kf_s \pm f_v| \tag{19}$$

Considering $\psi(t)$ definition, f_a is equal to 0, f_r or f_{cage} ($\omega_{cage}/2\pi$) respectively for the outer raceway, inner raceway and ball defects. Some interesting points are achieved by

This article has been accepted for publication in a future issue of this journal, but has not been fully edited. Content may change prior to final publication. Citation information: DOI 10.1109/TEC.2017.2758382, IEEE Transactions on Energy Conversion

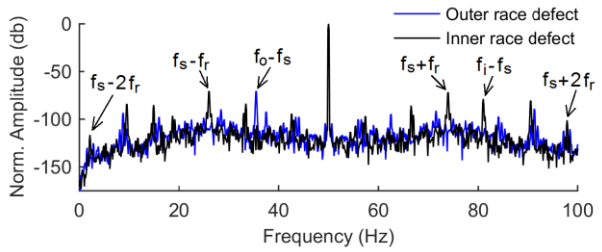

Fig. 9. Stator current normalized spectra obtained by simulation under the outer raceway and inner raceway defects with ρ=0.3 without magnetic saturation and inherent eccentricity effects.

careful examination of (18) and (19). For example, putting s=2 (including saturation), r=a=0 and k=2, i.e. for modulation of $2f_s \pm cf_{ch}$ harmonics of the stator inductances, which are produced by the similar harmonics in the inverse of the air gap function, to the 2nd harmonic of the stator current, the fault characteristic vibration frequencies and their integer multiples (cf_{ch}) can be present in the stator line current. This fact has been observed in [9] where $2f_i$ harmonic indicated in Fig. 10, but no reasoning has been given there. Also, putting s=k=2 and r=c=0, i.e. for modulation of $2f_s \pm af_a$ harmonics of the stator inductances to the 2nd harmonic of the stator current, af_a harmonics can be present in the stator line current. Considering definition of f_a for various bearing defects, this means that f_r and f_{cage} frequencies as well as their integer multiples can be presented in the stator current respectively for the inner raceway and ball defects. In addition, for the inner raceway defect where f_a=f_r, putting c=s=r=0, f_{cur} equals $|kf_s \pm af_r|$. These harmonics has been known as the main indices for the mixed eccentricity fault, thus, the bearing inner raceway defect can produce the same harmonics in the stator line current as the mixed eccentricity fault.

Fig. 9 shows the stator current spectra obtained by simulation for a 1.1 kW SCIM under the outer raceway and inner raceway defects without saturation and inherent eccentricity effects. The SCIM technical data is given in Table I in the next section. As already predicted, $f_s \pm f_r$ and $f_s \pm 2f_r$ frequencies are present only in the spectrum for the inner raceway defect. In addition, f_i-f_s and f_o-f_s frequencies are visible in the inner raceway and outer raceway defect conditions respectively. Fig. 10(a) and (b) offer similar simulation results under more practical conditions, i.e. under the outer raceway and inner raceway defects respectively by including saturation and inherent eccentricity effects. Also, to provide required condition for cf_{ch} and af_a frequencies to be present in the stator current spectra, a 2nd harmonic of 2% amplitude is added to the stator voltages. As seen, many harmonic components corresponding to (19) are present in the stator current spectra due to different factors, where some of them are indicated by arrows. For comparison purpose, two other charts are included in Fig. 10. Fig. 10(c)/(d) offer simulation results for the stator line current spectrum under the healthy condition with purely sinusoidal stator voltages, without inherent eccentricity and with/without saturation

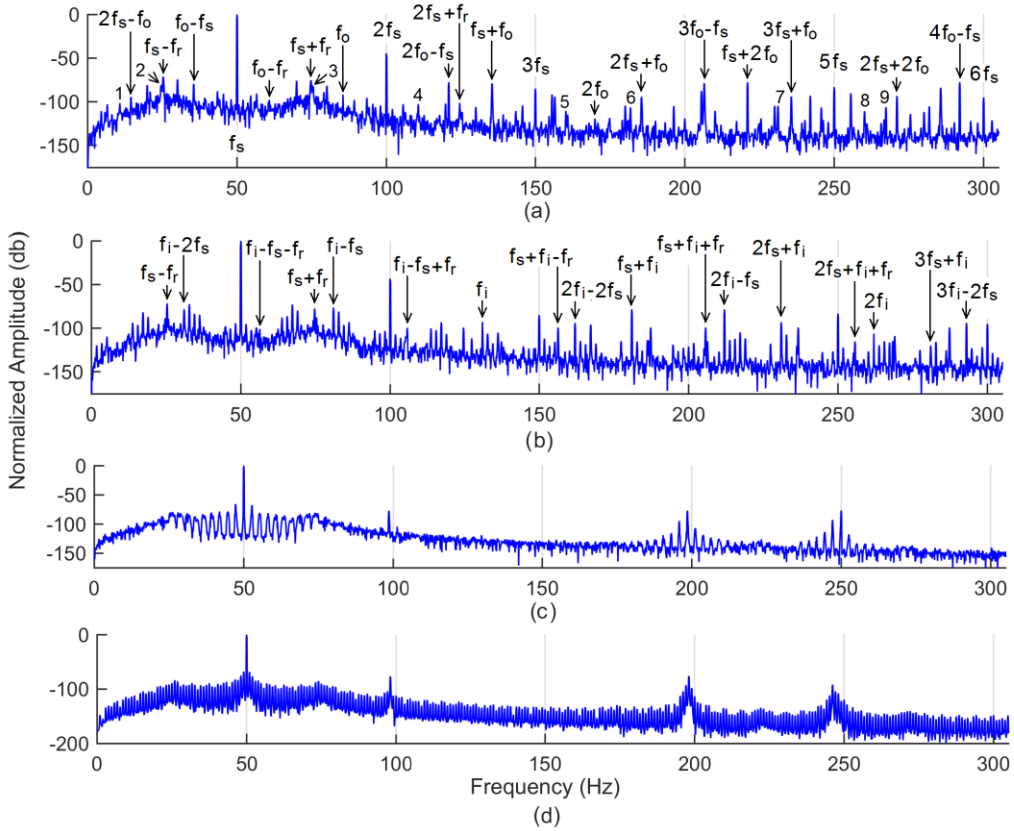

Fig. 10. Stator current normalized spectra obtained by simulation under: (a)/(b) outer raceway/inner raceway defect (ρ=0.3) with magnetic saturation, inherent eccentricity and 2nd harmonic of the stator voltages where the harmonics indicted by 1-9 in (a) are f_o-f_s-f_r, f_r, $2f_s$-f_r, f_o+f_s-f_r, f_o+f_s+f_r, $3f_o$-f_s-f_r, $3f_o$-f_s+f_r, f_o+$3f_s$+f_r and $4f_o$-f_s-f_r respectively, (c)/(d) healthy condition with/without saturation, with purely sinusoidal stator voltages and without inherent eccentricity

This article has been accepted for publication in a future issue of this journal, but has not been fully edited. Content may change prior to final publication. Citation information: DOI 10.1109/TEC.2017.2758382, IEEE Transactions on Energy Conversion

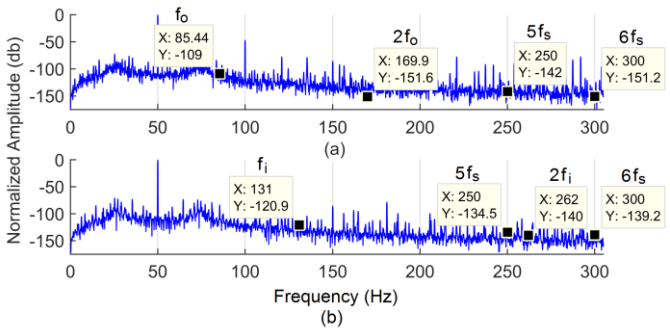

Fig. 11 (a) and (b) the stator current normalized spectra obtained by simulation under the same conditions as in Fig. 10 (a) and (b) but by excluding the magnetic saturation effect

effect. In addition to the fundamental frequency (50 Hz), Fig. 10(d) shows some frequency components near 100 Hz, 200 Hz and 250 Hz, whose presence are justified using the second part in right hand side of (10), where the rotor mesh currents are multiplied by the mutual inductances between the rotor meshes and the stator windings. As Fig. 4 shows, these mutual inductances are oscillating with a fundamental frequency of $pf_r/2$ or $(1\text{-}s)f_s$ and the rotor mesh currents contain sf_s frequency component (s is the slip). By including only the saturation effect, Fig. 10(c) shows some frequency components with small amplitudes created both sides the above-mentioned frequencies. These new frequencies are created by the new frequency components introduced in the rotor mesh currents due to the saturation effect. The harmonic content of the rotor mesh currents change considerably by including the bearing fault, inherent eccentricity and 2nd harmonic of the supply voltage, therefore, while many of the frequency components appeared in Fig. 10(c) are also present in Fig. 10(a) and (b), but they are not so clear because some new frequencies have been added among them and their amplitudes have been generally reduced. However, the presence of the 5th harmonic (250 Hz) with significant amplitude is a clear difference between Fig. 10(c) and (d), which is also discernible in Fig. 10(a) and (b). To clarify the main effects of the magnetic saturation on Fig. 10 (a) and (b), simulations are repeated at the same conditions, but without the saturation effect, and the resultant stator current spectra are presented in Fig. 11. As seen, the 5th harmonic as well as f_o, $2f_o$, f_i and $2f_i$ frequencies are eliminated from the spectra by excluding the saturation effect. The 2nd harmonic of the stator supply voltage along with the saturation effect produce the 6th harmonic in the spectra, which is also eliminated by excluding the saturation effect.

V. Experimental Verification

This section offers and compares the corresponding simulation and experimental results under the outer and inner raceway faults. An industrial 1.1 kW, 380 V, 50 Hz, three phase SCIM is considered for this purpose. Table I summarizes the technical data of the SCIM. The SCIM is equipped with ball bearing number 6205 at both ends. Local defects are created by drilling holes on the outer raceway and inner raceway of two different bearings as shown in Fig. 12.

TABLE I. Technical Data of SCIM

Parameter	Value
Nominal Power	1.1-kW
Nominal Voltage	380 V
Nominal Frequency	50 Hz
Connection	Y
Number of Poles	4
Rotor Slots Number	28
Stator Slots Number	36
Air gap Length	0.3 mm
Stack Length	75 mm
Air gap Mean Radius	40 mm
Stator winding turn per coil	63
Stator Resistance per phase	7.8-Ω
Rotor Bar Resistance	9.72 μΩ
End Ring Resistance	8-μΩ
Rotor Bar Leakage Inductance	0.571 μH
End Ring Leakage Inductance	0.051 μH
Inertia Moment	0.002385 gm^2
Rotor Bar Skewing Arc	10.92 Deg.
Winding scheme of phase A:	
A-1-12′-2-11′-3-10′-19-30′-20-29′-21-28′-X	

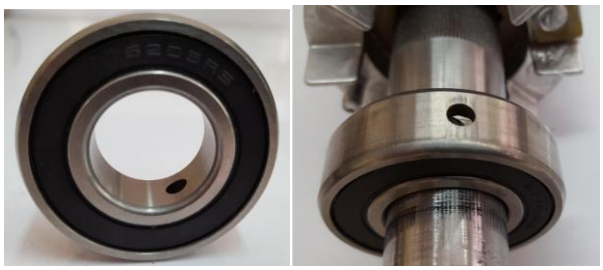

(a) (b)

Fig. 12. Photograph of the ball bearing with a hole on the: a) inner raceway, and b) outer raceway.

For the same bearing number, it has been shown in [13] that the fault related harmonics cannot be seen in the stator current spectrum with a hole of 3 mm diameter, but they become visible with a hole of 6 mm diameter. Here, the hole of 2 mm diameter was examined first, but satisfactory results were attained with the hole of 5 mm diameter. Our physical inspections show that the radial vibration amplitude have little increase by such increase of the hole diameter due to limited clearance between the bearing components, so, it seems that with smaller holes, the time width of the vibration pulses are so small that the related harmonic components in the stator current cannot grow up above the noise level. Defective bearings are replaced on the drive end of the rotor shaft in turn and the SCIM is run, while a data acquisition card of type PCI 1716 along with current sensors of type LTS6-NP and voltage sensors of type LV25-P are used for sampling and recording the stator line currents and voltages. The stator line current spectrum is attained by applying FFT to the sampled values. Fig. 13 shows the resultant spectra under the outer raceway defect as well as the healthy condition. Corresponding simulation results are also given in the figure. To bring the simulation conditions as close as possible to the corresponding experiments, in each case, the SCIM model is fed by the experimentally sampled stator voltages and a value of ρ=0.3 is applied. As seen, some frequency components corresponding

This article has been accepted for publication in a future issue of this journal, but has not been fully edited. Content may change prior to final publication. Citation information: DOI 10.1109/TEC.2017.2758382, IEEE Transactions on Energy Conversion

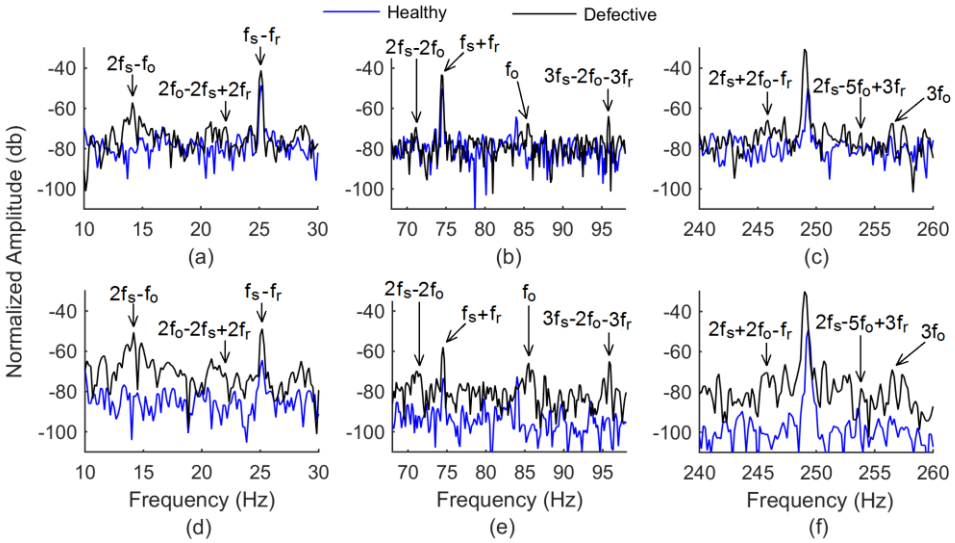

Fig. 13. The stator current normalized spectra at various frequency spans for the healthy and outer raceway fault conditions obtained through experiments (upper row) and simulations with ρ=0.3 (lower row).

to (19) are indicated on the spectra for the faulty case both in the experimental and simulation results. A small difference is permissible between the frequencies of the corresponding components in the simulation and experimental results, because f_o depends on the rotor speed: a quantity whose corresponding values obtained by the simulation and experiment may differ slightly due to the model imperfection. Except for f_s-f_r and f_s+f_r components, other indicated harmonics are directly rooted to the outer raceway defect, where some show considerable difference between the healthy and faulty cases. As seen, the experimental results approve in quality the corresponding simulation results. However, Fig. 13 shows amplification of the f_s-f_r and f_s+f_r components, while generation of these components by the outer raceway fault cannot be confirmed using (19). As Fig. 2(b) shows, the outer raceway fault produces repetitive temporary eccentricity at a fixed angle. The time average of the rotor center displacement along this angle may be considered as a continues static eccentricity component. Adding this component to the inherent eccentricity can amplify the proposed harmonic components.

Experiment and simulation are also performed on the SCIM under the inner raceway defect and the attained results along with the results for the healthy condition are compared in Fig. 14. To reach this qualitative comparison, the SCIM model is fed by the experimentally sampled stator voltages and the temporary eccentricity severity is set to 0.4 in simulation. Some harmonics predicted by (19) are indicated on the spectra for the faulty cases. As f_i is also dependent on the rotor speed, a small discrepancy is allowed between the frequencies of the corresponding components in the experimental and simulation results. As stated before, since f_a=f_r for the inner raceway defect, f_s-f_r and f_s+f_r harmonics are intensified by this fault. In the experimental spectrum of Fig. 13, the normalized amplitudes of these two harmonics are -41.11 dB and -43.20 dB respectively, while they are -37.35 dB and -37.82 dB in the experimental spectrum of Fig. 14, i.e. the inner raceway defect

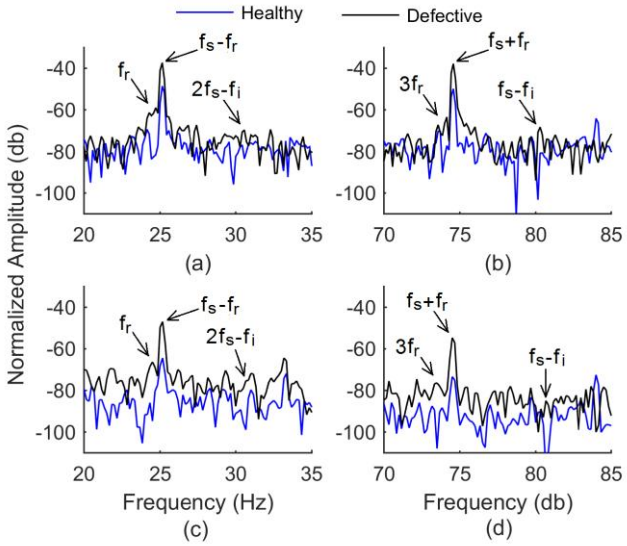

Fig. 14. The stator current normalized spectra at various frequency spans for the healthy and inner raceway fault conditions obtained through experiments (upper row) and simulations with ρ=0.4 (lower row).

have increased the normalized amplitudes of the harmonics by 3.76 dB and 5.38 dB respectively. Such increase of the amplitudes due to the inner raceway defect are 1.88 dB for f_s-f_r harmonic and 3.22 dB for f_s+f_r harmonic in the simulation results. Therefore, the inner raceway fault intensifies the amplitudes of the harmonics which are known previously as the main indices for the mixed eccentricity fault. Except for these two harmonics, the inner raceway fault usually produces weaker harmonic components.

VI. Conclusion

By defining appropriate air gap function, it is possible to use multiple coupled circuits modeling technique to achieve an analytic model for three-phase squirrel cage induction motors (SCIM) under localized defects of the roller bearings. Numerical Fourier analysis of the inverse air gap function by

including the saturation effect and inherent eccentricity shows that the vibration characteristic frequencies of the faults as well as the rotation frequencies of the temporary eccentricity caused by the bearing faults and their integer multiples (cf_{ch}, af_r and af_{cage}) can also be presented in the stator line current. Also, the bearing inner raceway defect can produce the same harmonics in the stator current as produced by the mixed eccentricity. Simulation results approve these facts and show some newly predicted frequency components in the stator line current spectrum under the bearing faults as well. This is verified by the experimental results, too. The proposed model is a helpful means to analyze and design non-invasive condition monitoring and fault diagnosis systems for the roller bearing faults within the SCIMs.

REFERENCES

[1] E. P. Cornell, E. L. Owen, J. C. Appiarius, R. M. McCoy, P.F. Albrecht, and D. W. Houghtaling, "Improved motors for utility applications," *Electric Power Reserch Institute*, Palo Alto, CA, vol. 1, no. 1763-1772, 1985.

[2] N. Tandon and A. Choudhury, "A review of vibration and acoustic measurement methods for the detection of defects in rolling element bearings," *International Journal of Tribology*, vol. 32, no. 8, pp. 469-480, Aug. 1999.

[3] W. T. Thomson, "A review of on-line condition monitoring techniques for three-phase squirrel cage induction motors—Past present and future," in *IEEE SDEMPED'99*, Spain, pp. 3–18, Sept. 1999.

[4] G.K. Singh, Sa'ad Ahmed Saleh Al Kazzaz, "Induction machine drive condition monitoring and diagnostic research- a survey," *Journal of electric power research*, vol. 64, pp. 145-158, Feb. 2003.

[5] S. Nandi, H. A. Toliyat, X. Li, "Condition monitoring and fault diagnosis of electrical motors - a review," *IEEE Trans. Energy Conversion*, vol. 20, no. 4, Dec. 2005.

[6] R. R. Schoen, T. G. Habetler, F. Kamran, R. G. Bartheld, "Motor bearing damage detection using stator current monitoring," *IEEE Trans. Industry Applications*, vol. 32, no. 6, pp. 1274-1279, Nov./Dec. 1995.

[7] M. E. H. Benbouzid, "A review of induction motors signature analysis as a medium for faults detection," *IEEE Trans. Industrial Electronics*, vol. 47, no. 5, pp. 984-993, Oct. 2000.

[8] M. E. H. Benbouzid, "What stator current processing-based technique to use for induction motor rotor faults diagnosis?" *IEEE Trans. Energy Conversion*, vol. 18, no. 2, pp. 238-244, Jun. 2003.

[9] M. Blodt, P. Granjon, B. Raison, and G. Rostaing, "Models for bearing damage detection in induction motors using stator current monitoring," *IEEE Trans. Industrial Electronics*, vol. 55, no. 4, pp. 1813 – 1822, April 2008.

[10] Valéria C. M. N. Leite, et. el, "Detection of localized bearing faults in induction machines by spectral kurtosis and envelope analysis of stator current," *IEEE Trans. Industrial Electronics*, vol. 62, no. 3, pp. 1855 – 1865, March 2015.

[11] S. E. Pandarakone, Y. Mizuno, and H. Nakamura, "Distinct fault analysis of induction motor bearing using frequency spectrum determination and support vector machine," *IEEE Trans. Industry Applications*, vol. 53, no. 3, pp. 3049-3056, May/Jun. 2017.

[12] F. B. Abid, S. Zgarni, A. Braham, "Bearing fault detection of induction motor using SWPT and DAG support vector machines," in *IECON 2016*, Florence, Italy, 2016, pp. 1476-1481.

[13] A. H. Boudinar, N. Benouzza, A. Bendiabdellah, M.-El-A. Khodja, "Induction motor bearing fault analysis using a Root-MUSIC method," *IEEE Trans. Industry Applications*, vol. 52, no. 5, pp. 3851-3860, Sep./Oct. 2016.

[14] E. Elbouchikhi, V. Choqueuse, Y. Amirat, M. E. H. Benbouzid, S. Turri, "An efficient Hilbert–Huang transform-based bearing faults detection in induction machines," *IEEE Trans. Energy Conversion*, vol. 32, no. 2, pp. 401-413, Jun. 2017.

[15] F. Immovilli, M. Cocconcelli, "Experimental investigation of shaft radial load effect on bearing fault signatures detection," *IEEE Trans. Industry Applications*, vol. 53, no. 3, pp. 2721-2729, May/Jun. 2017.

[16] M. He, D. He, "Deep learning based approach for bearing fault diagnosis," *IEEE Trans. Industry Applications*, vol. 53, no. 3, pp. 3057-3065, May/Jun. 2017.

[17] M. Ojaghi, N. Yazdandoost, "Oil-whirl fault modeling, simulation, and detection in sleeve bearings of squirrel cage induction motors," *IEEE Trans. Energy Conversion*, vol. 30, no. 4, pp. 1537-1547, Dec. 2015.

[18] M. Ojaghi, N. Yazdandoost, "Closure to discussion on oil-whirl fault modeling, simulation, and detection in sleeve bearings of squirrel cage induction motors," *IEEE Trans. Energy Conversion*, vol. 31, no. 4, pp. 1701-1702, Dec. 2016.

[19] F. Immovilli, C. Bianchini, M. Cocconcelli, A. Bellini, and R. Rubini, "Bearing fault model for induction motor with externally induced vibration," *IEEE Trans. Industrial Electronics*, vol. 60, no. 8, pp. 3408 – 3418, Aug. 2013.

[20] D. S. Vilchis-Rodriguez, S. Djurovic, and A. C. Smith, "Wound rotor induction generator bearing fault modelling and detection using stator current analysis," *IET Renewable Power Generation*, vol. 7, no. 4, pp. 330 – 340, July 2013.

[21] M. Ojaghi, and M. Sabouri "Dynamic modeling and simulation of induction motors with different bearing faults," in *ICEMS 2015*, Pattaya, Thailand, 2015.

[22] X. Luo, Yuefeng Liao, H. A. Toliyat, A. El-Antably, and A. lipo, "Multiple coupled circuit modeling of induction machines," *IEEE Trans. on Industry Applications*, vol. 31, no. 2, pp. 311 - 318, March-April. 1995

[23] J. Faiz, and I. Tabatabaei, "Extension of winding function theory for nonuniform air gap in electric machinery", *IEEE Trans. Magnetics*, vol. 38, no. 6, pp. 3654 - 3657, Nov. 2002

[24] B. Li, M. Chow, Y. Tipsuwan, and J. Hung, "Neural-network-based motor rolling bearing fault diagnosis," *IEEE Trans. Industrial Electronic*s, vol. 47, no. 5, pp. 1060–1069, Oct. 2000

[25] J. C. Moreira, and T. A. Lipo, "Modeling of saturated ac machines including air gap flux harmonic components," *IEEE Trans. Ind. Appl.*, vol. 28, pp. 343–349, Mar./Apr. 1992.

[26] M. Ojaghi, and J. Faiz, "Extension to multiple coupled circuit modeling of induction machines to include variable degrees of saturation effects," *IEEE Trans. Magn.*, vol. 44, no. 11, pp. 4053–4056, Nov. 2008.

[27] J. Faiz, and M. Ojaghi, "Stator inductance fluctuation of induction motor as an eccentricity fault index," *IEEE Trans. Magn.*, vol. 47, no. 6, pp. 1775–1785, June 2011.

Mansour Ojaghi (S'05, M'10) received his B.Sc. degree from Shahid Chamran University, Ahwaz, Iran in 1993, his M.Sc. degree from the University of Tabriz, Tabriz, Iran in 1997, and his Ph.D. degree from the University of Tehran, Tehran, Iran, in 2009 all in Electrical Engineering. He was with the Zanjan Regional Electricity Company for 10 years, where he held the position of Manager of Grid Technical Office. After receiving his Ph.D., Dr. Ojaghi joined the Department of Electrical Engineering, University of Zanjan, Zanjan, Iran, where he is currently working as an Associate Professor.

Dr. Ojaghi is a Member of the Power and Energy, Industrial Electronics, and Industry Applications Societies of the IEEE. His research interests include modeling, simulation, and fault diagnosis of electrical machines and drives as well as the power system protection.

Mahdi Sabouri was born in Zanjan, Iran in 1985. He received his B.Sc. and M.Sc. degrees both in electrical engineering in 2008 and 2012 respectively. Currently, he is a PHD candidate at Department of Electrical Engineering, University of Zanjan, Zanjan, Iran. His research interests include condition monitoring of induction motors, application of intelligent methods in power systems, distributed generation modeling, fault diagnosis of electric machines, analysis and design of electrical machines. He has published and presented about 20 papers in various journals and conferences in mentioned fields.

This article has been accepted for publication in a future issue of this journal, but has not been fully edited. Content may change prior to final publication. Citation information: DOI 10.1109/TEC.2017.2758382, IEEE Transactions on Energy Conversion

Professor Jawad Faiz (M'90, SM97) received his Master's degrees in electrical engineering from the University of Tabriz in Iran in 1975 graduating with First Class Honors. He received the Ph.D. degree in Electrical Engineering from the University of Newcastle upon Tyne, England in 1988. Early in his career, he served as a faculty member in the University of Tabriz for 10 years. After obtaining Ph.D. degree he rejoined the University of Tabriz where he held the position of Assistant Professor from 1988 to 1992, Associate Professor from 1992 to 1997, and has been a Professor since 1998. Since February 1999 he has been working as a Professor at School of Electrical and Computer Engineering, College of Engineering, University of Tehran. He is currently the Director of the Center of Excellence on Applied Electromagnetic systems. He has received a number of awards including the first basic research award from the Kharazmi International Festival in 2007, the silver Einstein medal for academic research from the UNESCO, the first rank medal in Research from the University of Tehran in 2006, the Elite Professor Award from the Iran Ministry of Science, Research and Technology in 2004, the Elite Professor of Iran National Elite Foundation (Allameh Tabatabei Award) in 2012, Life Researcher Award from IEEE Iran Section, 2015, author of the top 1% most highly cited papers in my field worldwide (1% Top Scientists in the World reported by ISI/ESI, Thomson Ruters ,2016, 2017).

He is the author of "Electronic Tap-changer for distribution transformers" book published in 2011 by Springer-Verlag and "Fault Diagnosis of Induction Motors" book published by IET in 2017. He published 230 papers in international journals and presented 247 papers in international conferences. Dr. Faiz is a Senior Member of Power Engineering, Industry Applications, Power Electronics, Industrial Electronics, Education and Magnetics Societies of the IEEE. He is also a member of Iran Academy of Science since 1999. His teaching and research interests are switched reluctance and VR motors design, design and modeling of electrical machines and drives, transformer modeling and design and fault diagnosis in electrical machinery and transformers.